Deep X-ray lithography on “sol–gel” processed noble metal mesoarchitectured films

Maxime Gayrard, Benedetta Marmiroli, Francois Chancerel, Philippe Decorse, Heinz Amenitsch, Jennifer Peron, Andrea Cattoni, Marco Faustini

COMMUNICATION

Deep X-Ray Lithography on "Sol-Gel" Processed Noble Metal Mesoarchitectured Films

Received 00th January 20xx,
Accepted 00th January 20xx

DOI: 10.1039/x0xx00000x

Maxime Gayrard,[a] Benedetta Marmiroli,[b] Francois Chancerel, [a,c,d] Philippe Decorse,[e] Heinz Amenitsch, [b] Jennifer Peron,[e] Andrea Cattoni,[c,d] and Marco Faustini [a*]

Noble metal coordination xerogels films (mesostructured with block-copolymers) exibit solubility switch with increasing X-ray irradiation. Differently from other sol-gel systems, this is attributed to the film deconstruction during irradiation. These materials can be used as recyclable negative tone resist for Deep X-Ray Lithography that can be further converted in metallic nanoarchitectured films.

Metallic nano- and microstructured films play a key role for the development of devices in a number of fields including electronics,[1, 2] photonics,[3] microfluidics,[4] electrochemistry[5] or (photo) catalysis.[6] Their integration into devices requires the development of patterning strategy of metallic materials. Among them, gold, silver (or even cost-less aluminum) have been widely explored. However, other noble metals (such as those of the platinum-group) are of particular interest because of their superior thermal and chemical stabilities, opening perspectives in emerging applications.[7] In electronics, metallic ruthenium films are used as a barrier for future-generation metal interconnects in logic devices and as a metal electrode for DRAM capacitors.[8, 9] Rhodium has recently gained attention in the field of ultraviolet (UV) plasmonics as O_2-resistant plasmonic photocatalyst.[10] Despite that, patterning strategies enabling integration into devices have not been reported (for Rh) or require multi-steps processes (for Ru).[1] In addition conventional processes are indirect, they rely on patterning of a sacrificial resist (polymer) followed by lift-off, electrodeposition and/or etching processes that can be very demanding for stable noble metals. Developing scalable and direct patterning strategies for noble metals would greatly simplify their integration in a number of devices. Besides polymeric resists, direct patterning was already demonstrated for Metal Organic Frameworks[11-14] or mesoporous oxides prepared by sol-gel process.[15-17] Among the various techniques, Deep X-Ray Lithography has proven to be very effective for the direct patterning of sol-gel precursors that were used as negative tone resists and further converted into oxides, typically by annealing.[17-20] For instance, X-Ray patterned Ti-based xerogels could be converted into crystalline TiO_2 by thermal treatment.[18] Generalizing the concept of "sol-gel process" beyond oxides by extending it to noble metals would enable direct patterning of metallic structures by X-Ray lithography. To do so, one must develop noble metal-based resists with two main requirements: (i) the resist should exhibit a solubility switch upon X-Ray exposure to allow for the development; (ii) the resist should directly be converted into metal by annealing. In addition, considering the high cost of the noble metal precursors, the process should be waste-free and should ideally allow for the recycling of the expensive resist by using environmental friendly solvents (such as H_2O). Here we show that mesostructured xerogels based on Ru and Rh (in presence of block-copolymers) act as effective negative tone resists for X-Ray lithography to obtain metallic nanostructures after annealing. Differently from previous reports on sol-gel derived transition metal oxides, we report for the first time on the radiation chemistry of underexplored "sol-gel" of noble metals. The key advantage of this "sol-gel" approach is that the materials can be shaped as polymeric resists by solution processing but can eventually be converted into metals. The general patterning strategy for noble metal xerogels is illustrated in Figure 1(a). The resist films are obtained from solutions containing the noble metal precursors (chlorides) and, a block-copolymer Pluronic F127. Differently from other noble metals chlorides such as gold, silver, platinum or palladium (that recrystallize after evaporation), in presence of block-copolymers Ru or Rh chlorides form homogenous films of optical quality after dip-coating (Figure S1). The dip-coating method is a waste free deposition technique, an important feature in case of costly noble metal precursors.[21] The film is then exposed to a synchrotron X-Ray radiation through a mask that induces a solubility change: the

[a.] *Sorbonne Université, CNRS, Laboratoire Chimie de la Matière Condensée de Paris (LCMCP), F-75005 Paris, France*
[b.] *Institute of Inorganic Chemistry, Graz University of Technology, Graz, Austria*
[c.] *Institut Photovoltaïque d'Ile-de-France (IPVF), CNRS UMR 9006, Palaiseau, France*
[d.] *Centre de Nanosciences et de Nanotechnologies (C2N), CNRS UMR 9001, Université Paris-Saclay, Palaiseau, France.*
e Université de Paris, ITODYS, CNRS, UMR 7086, 15 rue J-A de Baïf, F-75013 Paris, France
Electronic Supplementary Information (ESI) available: See DOI: 10.1039/x0xx00000x

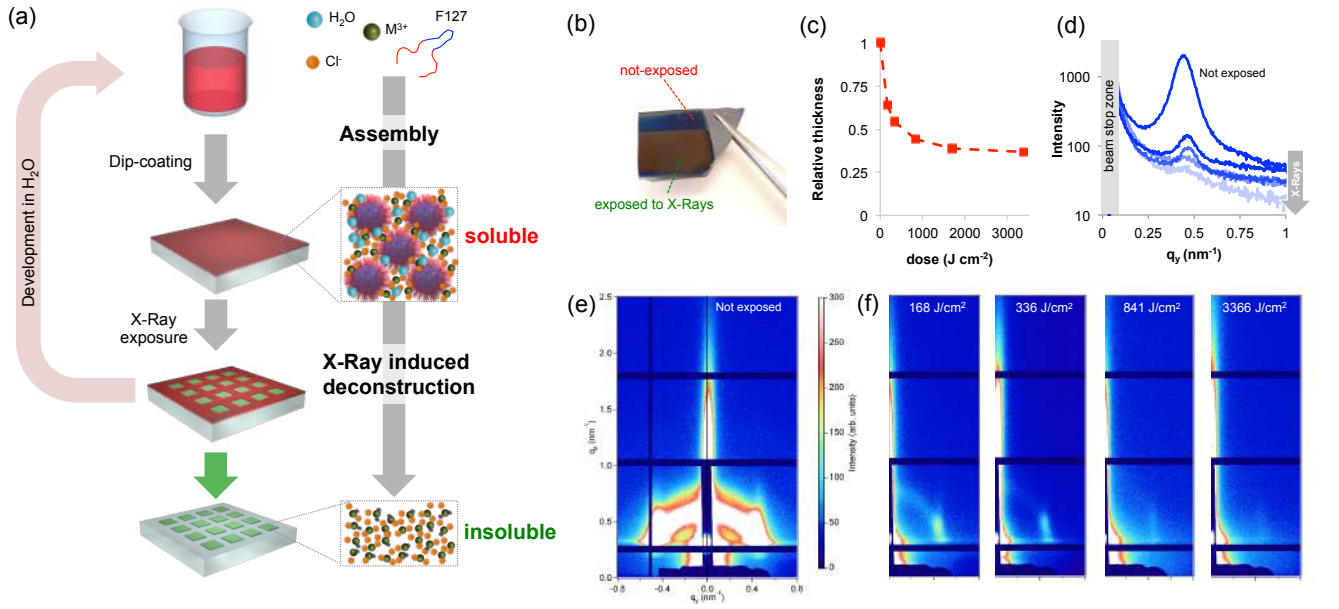

Figure 1 (a) Illustration of the patterning strategy of noble metal mesostructured xerogels. (b) Photograph of a Ru-based xerogel partially exposed to X-Ray radiation. (c) Evolution of the relative thickness of a $RuCl_3$/F127 xerogel as function of the X-Ray dose. (d) Evolution of the scattering intensity as function of the qy for samples exposed to increasing doses. (e) GI-SAXS pattern of the unexposed $RuCl_3$/F127 xerogel and, (f) evolution of GI-SAXS pattern of the sample at increasing exposure doses.

exposed materials become insoluble in polar solvents. The non-exposed material is developed in water. Water is also one of the solvents of the initial solution, and this is a key condition for the recycling of the initial noble metal precursors. The patterned insoluble materials can be annealed in reducing atmosphere (H_2 at 300°C) and directly converted in the corresponding noble metal.

A detailed study on structural and chemical evolution of the materials induced by the X-Ray exposure is presented for the case of Ru-based films. We first discuss the evolution of the structure. As in classical sol-gel process, self-assembly during evaporation (during the dip-coating step) results in the formation mesostructured hybrid materials composed of organic micelles surrounded by amorphous metallic complexes.[16] This was confirmed by GI-SAXS on a $RuCl_3$/F127 film before exposure (Figure 1e). GI-SAXS measurement of the non-exposed material shows the characteristic diffraction pattern of the Im3m mesostructure (body center cubic arrangement).[17] After X-Ray exposure, in all the cases, a colour difference between the exposed and unexposed zones (latent image) is already visible by naked eye as exemplified in the optical photograph in Figure 1(b). The colour difference can be attributed to a structural modification of the films (such as a thickness decrease). We thus investigated in detail the effect of the X-Ray radiation dose on the structural properties of the films by UV-visible spectroscopic ellipsometry and GI-SAXS. The evolution of the relative thickness vs dose is shown in Figure 1(c). For all the films investigated hereafter, the initial thickness was around 100 nm. The relative thickness already significantly decreases at low doses and progressively reaches a contraction of 66% at higher doses. This decrease in thickness is characteristic of a densification of the material due to the X-Ray radiation. The densification can be due to the water loss or/and polymer degradation. The same study was performed for $RuCl_3$ films without F127 (Figure S2) and already at moderate exposure doses, $RuCl_3$ films exhibit a contraction of 30%-33%. This decrease can therefore be indeed attributed to the partial loss adsorbed water (more details will be shown later on). To gain better understanding, the evolution of the mesostructure after exposure at increasing doses was investigated by GI-SAXS (Figure 1f). The characteristic diffraction signal of the unexposed film progressively disappears upon X-Ray irradiation; we integrated the signal intensity along the in-plane 1-10 direction as a function of X-Ray dose (Figure 1d). The diffraction signal at q_y= 0.42 nm^{-1} corresponds to a d-spacing of 14.9 nm which is in agreement with mesostructures containing F127 micelles. The strong decrease of the intensity already a low doses indicates a loss of the mesostructure, likely due to a chemical modification of the block-polymer micelles.[22]

The chemical evolution during exposure was investigated by (i) GI-WAXS and XPS to characterized the noble metal precursor and (ii) infrared (IR) spectroscopic ellipsometry to probe the evolution of the polymer and H_2O. The chemical evolution of the inorganic precursor vs X-Ray irradiation was first characterized by GI-WAXS. As shown in Figure S3, the GI-WAXS

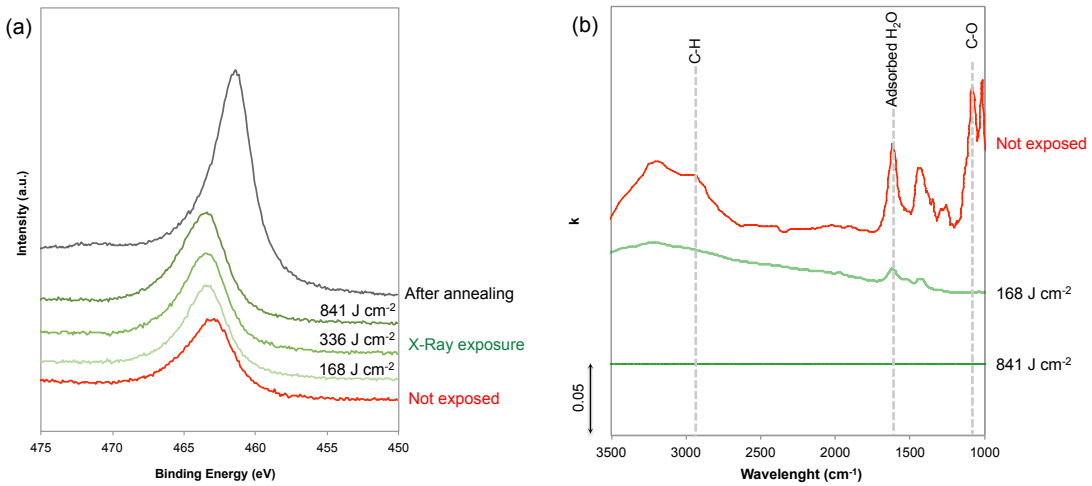

Figure 2 (a) XPS spectra recorded in the Ru(3p) region on films exposed at different doses and annealed in reducing atmosphere. (b) Evolution of the extinction coefficient k of a $RuCl_3$/F127 film before and after exposure at different doses.

patterns do not present any characteristic diffraction peak indicating that the Ru based xerogels are amorphous. To gain better understanding, the evolution of Ru, O and Cl oxidation states upon exposure were probed by XPS (Figure 2a and Figure S4). Since Ru(3d) core levels superimpose the C(1s) core level, the Ru(3p) region was analyzed. From Ru(3p) spectra plotted on Figure 2(a), we can see that Ru(3p) does not shift upon exposure time and remains at 463.1 eV, which is characteristic of Ru(III) species. Interestingly, the Cl/Ru for non-exposed sample is ~3 confirming that the film presents a stoichiometry close to the initial precursor $RuCl_3$ in agreement with previous reports.[23, 24] Before exposure, noble metal precursors, that can be formally described as $Ru(Cl)_x(OH)_y$, are likely coordination xerogel based mostly on Cl ligands.[25] The peaks characteristic of the Cl 2p3/2 and 2p1/2 also remain located at 197.8 and 199.3 eV upon exposure (Figure S4), however a progressive decrease in Cl/Ru ratio is observed with increasing exposure time. The Cl/Ru decreases from ~3 for non-exposed sample, down to 2.53, 1.46 and 0.71 with exposure doses of 168, 336 and 841 respectively. .This decrease of Cl content can be attributed to the formation of more hydroxylated species (-OH). XPS spectra in the O1s region (Figure S4) confirms the presence of H_2O in non-exposed samples, with the O(1s) peak centered at 533 eV. Upon exposure, the contribution of water into the O(1s) peak disappears and the O(1s) peak is shifted to 531.5 eV which is characteristic of hydroxylated species. In contrast, no peaks centered at 529.3 eV characteristic of the M-O-M bond are observed. [23] This suggests that, differently from other sol-gel systems, the X-Ray irradiation does not promote condensation in the case of Ru.

We then perfomed IR ellipsometry as shown in Figure 2(b). During an ellipsometric experiment, IR polarized light beam interacts with the film. This interaction changes the state of polarization of the reflected light which may be parametrized by the interference amplitude component Ψ and the phase difference Δ. Both Ψ and Δ values are very sensitive to photons absorptions due to vibrational modes at IR wavelengths. The Ψ and Δ spectra are then analyzed by the software "IR Wase" to obtain refractive index (n) and extinction coefficient (k) of the films. Figure 2(b) shows the evolution of k as function of wavelength for Ru-based films before and after X-Ray exposure. Before exposure, the $RuCl_3$/F127 film shows many different features: the bands centered between 1650-1670 cm^{-1} and between 3200-3400 cm^{-1} can be attributed to the presence of water molecules in the film, due to residual water from the initial solution and/or due to humidity from the atmosphere.[26] The large O-H band at 3200-3400 cm^{-1} partially overlaps in the range 2850-2920 cm^{-1} with the CH_2 symmetric and asymmetric stretching bands of Pluronic F127. The band at ca. 1100 cm^{-1} can be attributed to the stretching of the C-O-C bonds in the PEO.[26 27] To confirm that, the k spectra of films of $RuCl_3$ and F127 (non-exposed) are also reported in Figure S5. After exposure at a low dose of 168 J-cm^2, the drastic decrease of the O-H bands confirms the partial water loss while the characteristic peaks of the polymers are not visible. At high dose 841 cm^{-2}, the raw ellipsometric spectra do not present any visible absorption peak and are thus fitted with a Cauchy model for not absorbing materials (k=0). It is important to mention that the presence of residual polymer or water might fall below of the detection limit of the IR ellipsometer. However, it is reasonable to propose that X-Ray induces deconstruction of the film with two main effects: (i) loss of the mesostructure (as observed by GI-SAXS) that can be attributed to the fact that high energy X-Ray radiation provokes complete decomposition of F127[22]; (ii) loss of the adsorbed water in agreement with the UV-vis ellipsometric analysis (Figure S2) and formation of hydroxocomplexes. What observed in this study is in agreement with the previous literature on sol-gel derived films. [28] The hard X-rays exposure to as-deposited sol–gel films produces hydrolysis of the precursors that is promoted by formation of free radicals. The free radicals H°

and OH° are formed by dissociation of water molecules exposed to X-Ray radiation. Residual water is indeed always present in the hybrid films containing F127 and the hydrated noble metal precursors. Free radicals are also responsible of the decomposition of the organic matter in the films.[28]

The film deconstruction during X-Ray exposure was also observed in the case of $RhCl_3$ films templated with F127. Figure 3 shows the evolution of the relative thickness as function of the dose. As observed for Ru, the Rh-based films contract progressively (up to 62% at high values of dose) attributed to water loss and decomposition of F127. The loss of the mesostructure is also confirmed by the selected GI-SAXS patterns in the inset of Figure 3. The progressive decrease of the GI-SAXS signal is in agreement with the mechanism described for Ru-based films.

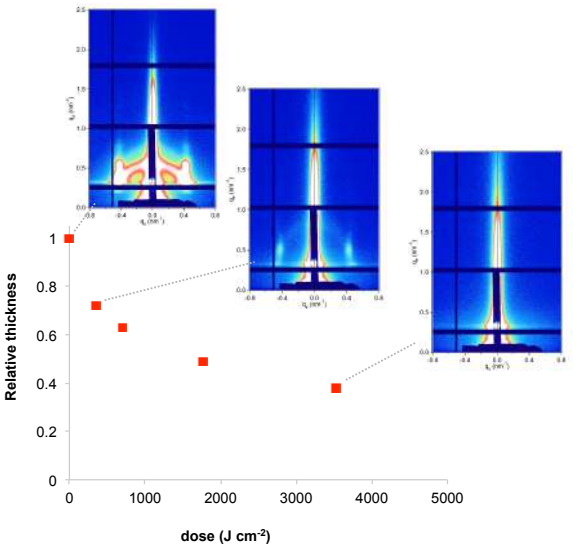

Figure 3 Evolution of the relative thickness of $RhCl_3$/F127 films as function of X-Ray dose. In the inset: corresponding GI-SAXS patterns

Coming back to the lithographic process, the combination of polymer decomposition, dehydration and partial hydroxylation is responsible of the solubility switch of the films. As mentioned above, to obtain an efficient negative tone resist for lithography, the exposed material must be insoluble while the unexposed material must be dissolved. The solubility contrast is thus crucial for the development step. We have tested the effectiveness of the development process on samples patterned through a mask. Examples of patterned samples before development are shown in Figure S6. The development step consisted in dipping the samples in H_2O for about 30 s; the quality of the micropatterns was then evaluated by optical microscopy. The table in Figure 4(a) summarizes the results of the development for the two metal precursors Ru, Rh chlorides alone or in presence of block-copolymers (F127) as function of the exposure doses. Several general trends can be observed. For all the systems, at low doses, the development is not efficient since the exposed material can re-dissolved in H_2O. Oppositely, for high doses (that imply very long exposure time) the development is not optimal: overexposure induces a modification also in the unexposed material at the pattern edge that becomes less soluble after irradiation. Films made of $RuCl_3$ and $RhCl_3$ without F127 become insoluble too after irradiation. This is not surprising since more hydroxylated Ru complexes present poor solubility in water.[29] However, without F127, the solubility contrast (between the exposed and the unexposed zones) is not high enough to achieve effective development in H_2O. For the $RuCl_3$/F127 and $RhCl_3$/F127 materials, 841 J-cm^2 is the optimal X-Ray dose to obtain an effective development in our conditions as exemplified in the optical micrographs in Figure 4(b) and 4(c). Similarly, the samples exposed at 841 J-cm^2 could be developed in other polar solvents such as ethanol (Figure S7). After development, the patterned noble metal xerogels can be converted into the respective metal by an annealing at 300°C under reducing atmosphere (H_2/Ar) as illustrated in Figure 5(a). XPS analysis in Figure 2 (a) of the film after annealing shows a Ru(3p) signal characteristic of Ru(0) species at 461.3 eV. SEM micrographs in Figure 5(b), (c), (d) and (e) show some examples of micropatterned Ru and Rh films obtained after annealing and exposure at 841 J-cm^{-2} on resists containing F127. A higher magnification SEM micrograph of the pattern's edge is shown in Figure S8. EDX mapping (insets of Figure 5) on single features indicate that only the metal is present without significant presence of O, Cl or N (not shown). SEM micrographs in the inset (Figure 5c and d) show that the metallic films fabricated by sol-gel process are

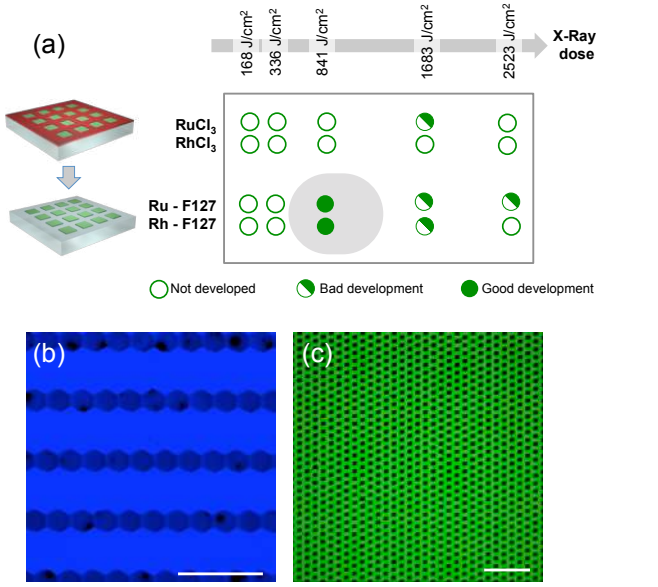

Figure 4 (a) Table summarizing the results of the development for the two metal precursors Ru, Rh chlorides alone or in presence of block-copolymers (F127) as function of the exposure doses (b) and (d) Falsed colored optical micrographs of the developed Rh and Ru-based resists respectively (scale bare 100 µm)

not dense but present porous nanoarchitectures. Indeed, during the reduction process, Cl/OH ligands are decomposed resulting in films that are composed by metallic nanoparticles forming a percolated network with voids. The formation of percolated nanoparticle layers (rather than isolated particles) is important for ensuring the metallic properties of the films (electrical and optical). To confirm, the optical properties of the films before and after reductive annealing have been probed by UV-vis spectroscopic ellipsometry.

Ray Lithography. The effect of the X-Ray radiation on the structure and chemical composition of the films was investigated by a set of techniques including GI-SAXS, Uv-vis and IR ellipsometries. Differently for other sol-gel based materials, no condensation take place but the X-Ray radiation induces the destructuration of the noble metal xerogels. We propose that block-copolymer decomposition, dehydration and partial hydroxylation are responsible for the solubility switch observed in the xerogels. We demonstrate that noble

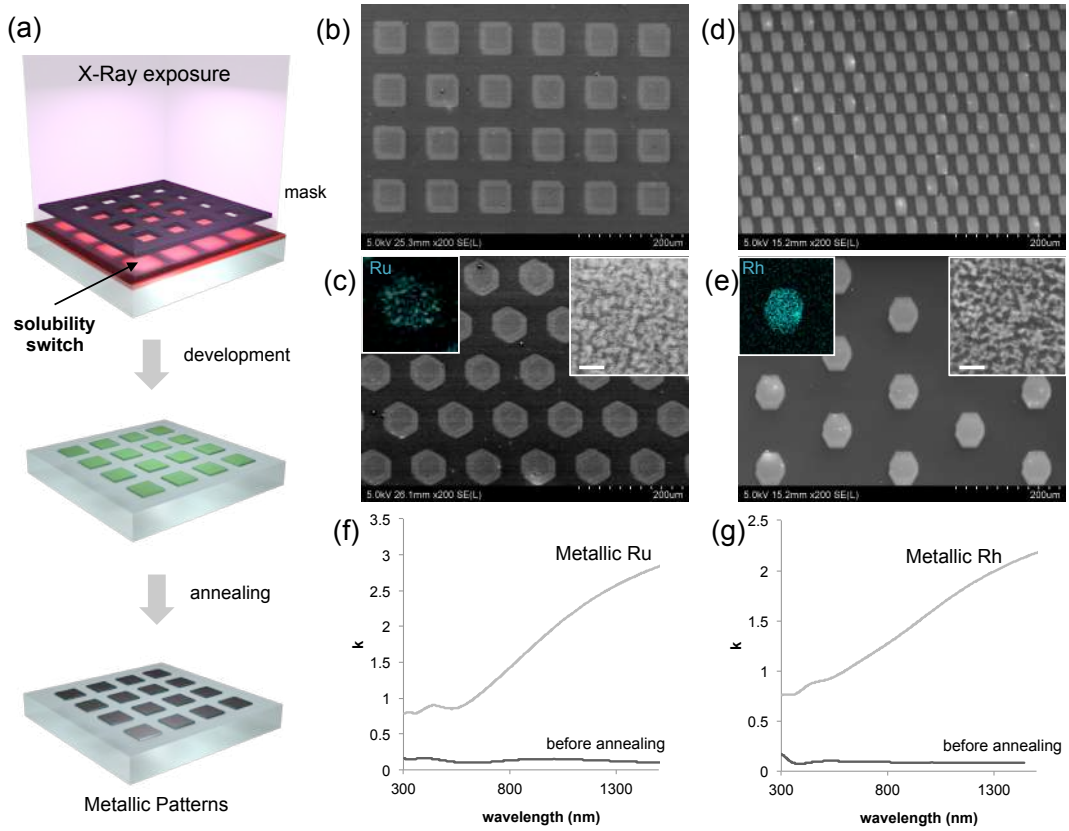

Figure 5 (a) Illustration of the lithographic process toward metallic patterns; SEM micrographs of (b) (c) Ru and (d) and (e) Rh patterns. The corresponding EDX mapping and higher resolution view are reported in the inset (scale bar 50 nm). (f) and (g) Evolution of the extinction coefficient k for Ru and Rh-samples before and after annealing

The plots in Figure 5 (f) and (g) display the evolution of k as a function of the wavelength for Ru and Rh, respectively. In both cases, before annealing (after exposure at 841 J cm^{-2}) the film presents low values of k, especially at low wavelength in the visible range that are attributed to the presence of colored Ru and Rh complexes in the films. After reductive annealing, the value of k drastically increases especially in the near infrared region; this behavior is characteristic of the formation of metallic conducting films.

Conclusions

In conclusion, we demonstrated that, for the first time, sol-gel processed mesostructured xerogels composed on noble metal precursors (Ru and Rh-based) act as negative tone resists for X-metal xerogels can directly be patterned by X-Ray lithography and converted into the corresponding metal by annealing. The process presents several advantages: it enables direct patterning and it minimizes wastes of the expensive noble metal precursors. Notably the development step is performed in water, a key requirement for the possible recycling of the resist. While in the present work we demonstrated the fabrication of micrometric patterns, DXRL theoretically enables patterning at the sub-micrometric scale. We believe that this report will trigger new fundamental research on X-ray assisted synthesis of nanostructured materials providing new possibilities for device fabrication at low cost. From a fundament point of view, this work expands the synthetic toolbox of sol-gel processed materials toward metals. We also provide new understanding in the radiation chemistry of noble

metal materials, a relatively underexplored field that is also of high interest for a broader community working in catalysis and electrocatalysis. As a future research line, it would be interesting to investigate if and how the X-ray radiation is influencing the catalytic properties of the noble metal films.

Acknowledgements

This work was supported by French state funds managed by the National Research Agency (ANR) through the MetaFleSS project, grant no. ANR-17-CE09-0027. M.F. acknowledges funding from the European Research Council (ERC) under European Union's Horizon 2020 Program (Grant Agreement no. 803220, TEMPORE). This project has also received funding from the EU-H2020 research and innovation program under grant agreement No. 654360 having benefitted from the access provided to ELETTRA Trieste, Italy, within the framework of the NFFA-Europe Transnational Access Activity. The infrared ellipsometry was funded by the Région Ile-de-France in the framework of DIM ResPore and by the French state within the Investissements d'Avenir programme under reference ANR-11-IDEX-0004-02, within the framework of the Cluster of Excellence MATISSE. The XPS KAlpha+ was funded by the Région Île-de-France (convention SESAME n°16016303). ANR (Agence Nationale de la Recherche) and CGI (Commissariat à l'Investissement d'Avenir) are also gratefully acknowledged for their financial support through Labex SEAM (Science and Engineering for Advanced Materialsand devices), ANR-10-LABX-096 and ANR-18-IDEX-0001. We thank D. Montero and the Institut des Matériaux de Paris Centre (IMPC FR2482) for servicing FEGSEM & EDX instrumentation and Sorbonne Université, CNRS and C'Nano projects of the Région Ile-de-France for funding.

Conflicts of interest

There are no conflicts to declare.

Notes and references

1. A. Mallavarapu, P. Ajay, C. Barrera and S. V. Sreenivasan, *ACS Applied Materials & Interfaces*, 2021, 13, 1169-1177.
2. M. Grobis, C. Schulze, M. Faustini, D. Grosso, O. Hellwig, D. Makarov and M. Albrecht, *Applied Physics Letters*, 2011, 98.
3. H.-L. Chen, A. Cattoni, R. De Lépinau, A. W. Walker, O. Höhn, D. Lackner, G. Siefer, M. Faustini, N. Vandamme and J. Goffard, *Nature Energy*, 2019, 4, 761-767.
4. H.-I. Ryoo, J. S. Lee, C. B. Park and D.-P. Kim, *Lab on a Chip*, 2011, 11, 378-380.
5. B. Jiang, C. Li, H. Qian, M. S. A. Hossain, V. Malgras and Y. Yamauchi, *Angewandte Chemie International Edition*, 2017, 56, 7836-7841.
6. Y. Gutiérrez, R. Alcaraz de la Osa, D. Ortiz, J. M. Saiz, F. González and F. Moreno, *Applied Sciences*, 2018, 8, 64.
7. R. J. Seymour and J. O'Farrelly, in *Kirk-Othmer Encyclopedia of Chemical Technology*, DOI: https://doi.org/10.1002/0471238961.1612012019052513.a01.pub3, pp. 1-37.
8. L. G. Wen, C. Adelmann, O. V. Pedreira, S. Dutta, M. Popovici, B. Briggs, N. Heylen, K. Vanstreels, C. J. Wilson and S. Van Elshocht, 2016.
9. T. N. Arunagiri, Y. Zhang, O. Chyan, M. El-Bouanani, M. J. Kim, K. H. Chen, C. T. Wu and L. C. Chen, *Applied Physics Letters*, 2005, 86, 083104.
10. A. M. Watson, X. Zhang, R. Alcaraz de la Osa, J. M. Sanz, F. González, F. Moreno, G. Finkelstein, J. Liu and H. O. Everitt, *Nano Letters*, 2015, 15, 1095-1100.
11. O. Dalstein, D. R. Ceratti, C. Boissière, D. Grosso, A. Cattoni and M. Faustini, *Advanced Functional Materials*, 2016, 26, 81-90.
12. M. Tu, B. Xia, D. E. Kravchenko, M. L. Tietze, A. J. Cruz, I. Stassen, T. Hauffman, J. Teyssandier, S. De Feyter and Z. Wang, *Nature Materials*, 2021, 20, 93-99.
13. M. Faustini, *Nature Materials*, 2021, 20, 8-9.
14. O. Dalstein, E. Gkaniatsou, C. Sicard, O. Sel, H. Perrot, C. Serre, C. Boissière and M. Faustini, *Angewandte Chemie International Edition*, 2017, 56, 14011-14015.
15. A. Cattoni, D. Mailly, O. Dalstein, M. Faustini, G. Seniutinas, B. Rösner and C. David, *Microelectronic Engineering*, 2018, 193, 18-22.
16. M. Faustini, C. Boissiere, L. Nicole and D. Grosso, *Chemistry of Materials*, 2014, 26, 709-723.
17. M. Faustini, M. Vayer, B. Marmiroli, M. Hillmyer, H. Amenitsch, C. Sinturel and D. Grosso, *Chemistry of Materials*, 2010, 22, 5687-5694.
18. M. Faustini, B. Marmiroli, L. Malfatti, B. Louis, N. Krins, P. Falcaro, G. Grenci, C. Laberty-Robert, H. Amenitsch, P. Innocenzi and D. Grosso, *Journal of Materials Chemistry*, 2011, 21, 3597-3603.
19. P. Falcaro, L. Malfatti, L. Vaccari, H. Amenitsch, B. Marmiroli, G. Grenci and P. Innocenzi, *Advanced Materials*, 2009, 21, 4932-4936.
20. L. Malfatti, D. Marongiu, S. Costacurta, P. Falcaro, H. Amenitsch, B. Marmiroli, G. Grenci, M. F. Casula and P. Innocenzi, *Chemistry of Materials*, 2010, 22, 2132-2137.
21. D. R. Ceratti, B. Louis, X. Paquez, M. Faustini and D. Grosso, *Adv. Mater.*, 2015, 27, 4958-+.
22. P. Innocenzi, T. Kidchob, S. Costacurta, P. Falcaro, B. Marmiroli, F. Cacho-Nerin and H. Amenitsch, *Soft Matter*, 2010, 6, 3172-3176.
23. M. Gayrard, J. Voronkoff, C. Boissière, D. Montero, L. Rozes, A. Cattoni, J. Peron and M. Faustini, *Nano Letters*, 2021, DOI: 10.1021/acs.nanolett.1c00178.
24. S. Duran, M. Elmaalouf, M. Odziomek, J.-Y. Piquemal, M. Faustini, M. Giraud, J. Peron and C. Tard, *ChemElectroChem*, 2021, 8, 3519-3524.
25. M. Odziomek, M. Bahri, C. Boissière, C. Sanchez, B. Lassalle-Kaiser, A. Zitolo, O. Ersen, S. Nowak, C. Tard, M. Giraud, M. Faustini and J. Peron, *Materials Horizons*, 2019, DOI: 10.1039/C9MH01408J.
26. R. M. Silverstein and G. C. Bassler, *Journal of Chemical Education*, 1962, 39, 546.
27. K. Pielichowski and K. Flejtuch, *Journal of Analytical and Applied Pyrolysis*, 2005, 73, 131-138.

28. P. Innocenzi, L. Malfatti and P. Falcaro, *Soft Matter*, 2012, 8, 3722-3729.
29. I. Povar and O. Spinu, *Journal of Electrochemical Science and Engineering*, 2016, 6, 145-153.